International Journal of Fluid Mechanics & Thermal Sciences
2017; 3(3): 25-31
http://www.sciencepublishinggroup.com/j/ijfmts
doi: 10.11648/j.ijfmts.20170303.11
ISSN: 2469-8105 (Print); ISSN: 2469-8113 (Online)

Boundary Layer Stagnation-Point Flow of Micropolar Fluid over an Exponentially Stretching Sheet

Abdul Rehman, Naveed Sheikh

Department of Mathematics, University of Balochistan, Quetta, Pakistan

Email address:
abdul_maths@yahoo.com (A. Rehman)

To cite this article:
Abdul Rehman, Naveed Sheikh. Boundary Layer Stagnation-Point Flow of Micropolar Fluid over an Exponentially Stretching Sheet. *International Journal of Fluid Mechanics & Thermal Sciences.* Vol. 3, No. 3, 2017, pp. 25-31. doi: 10.11648/j.ijfmts.20170303.11

Received: May 19, 2017; **Accepted**: August 24, 2017; **Published**: October 7, 2017

Abstract: In this paper, the steady boundary layer stagnation point flow and heat transfer of a micropolar fluid flowing over an exponentially stretching sheet is investigated. The solution of the problem is obtained numerically using the Keller-box method and the series solutions are obtained with the help of homotopy analysis method (HAM). Comparisons of both the solutions are presented. At the end the effects of important physical parameters are presented through graphs and the salient features are discussed.

Keywords: Boundary Layer Flow, Heat Transfer, Micropolar Fluid, Exponential Stretching/Shrinking, Keller-Box Scheme, Homotopy Analysis Method

1. Introduction

The study of stretching sheet was initiated by Crane [1], has attained lot of attention due to its wide range of engineering applications. Literature is rich of the material concerning the boundary layer flow of steady/unsteady flow of Newtonian/non-Newtonian fluids. In a recent paper Merkin and Kumaran [2] has studied the unsteady boundary layer flow on a shrinking surface in an electrically conducting fluid. Moreover, the suction effects for the magneto hydrodynamic viscous flow over a shrinking sheet have been analyzed by Akyildiz and Siginer [3]. According to their analysis the velocity field exhibited a decreasing behavior with respect to the suction parameter. The problem of stagnation point flow of a viscous fluid towards a stretching sheet was discussed analytically by Nadeem et al. [4]. Further, the steady boundary layer stagnation point flow of a micropolar fluid towards a horizontal linearly stretching/shrinking sheet has been studied by Yacob et al. [5]. They solved the problem numerically using the Runge-Kutte-Fehhlberg method with shooting technique. Nadeem and Awais [6] have examined the effects of variable viscosity and variable thermo capillarity on the unsteady flow in a thin film on a horizontal porous shrinking sheet through a porous medium. Moreover, the stagnation point flow towards a shrinking sheet has been analyzed by Wang [7], the obtained results were reflecting that a region of reverse flow occurs near the surface and that for larger shrinking rates, the solution/similarity can't be obtained. Recently, the suction/blowing and thermal radiation effects on steady boundary layer stagnation point flow and heat transfer over a porous shrinking sheet has been investigated by Bhallacharrya and Layek [8].

The study of stretching/shrinking sheet phenomena for the boundary layer stagnation point flow has been considered by many researchers for linear/polynomial stretching but not a lot of work is available on these concepts with exponential stretching and stagnation point flow. Recently, Abdul Rehman et al. [9] have presented the solutions for the problem of boundary layer flow and heat transfer of a third grade fluid flowing over an exponentially stretching sheet. In another attempt, Abdul Rehman et al. [10] have also discussed the nanoparticles effect over the boundary layer flow of a Casson fluid flowing over an exponentially stretching surface. The purpose of the present work is to provide a solution of the boundary layer stagnation point flow of a micropolar fluid for exponentially stretching/shrinking sheets. The solutions are obtained through a second order difference scheme known as the Keller-box technique. Also the analytical solutions are obtained by using the homotopy analysis method (HAM). Comparisons of both the solutions are presented for

compatibility. Details about the homotopy analysis method can be found in Refs. [11-28].

2. Formulation

Let us consider a stagnation point flow of an incompressible micropolar fluid over an exponentially stretching sheet. The Cartesian coordinates *(x, y)* are used such that *x* is along the surface of the sheet, while *y* is taken as normal to it. The related boundary layer equations of motion in the presence of microrotation and heat transfer are

$$\frac{\partial u}{\partial x}+\frac{\partial v}{\partial y}=0, \tag{1}$$

$$u\frac{\partial u}{\partial x}+v\frac{\partial u}{\partial y}=U_\infty\frac{dU_\infty}{dx}+\left(\nu+\frac{k}{\rho}\right)\frac{\partial^2 u}{\partial y^2}+\frac{k}{\rho}\frac{\partial u}{\partial y}, \tag{2}$$

$$\rho j\left(u\frac{\partial N}{\partial x}+v\frac{\partial N}{\partial y}\right)=\gamma\frac{\partial^2 N}{\partial y^2}-k\left(2N+\frac{\partial u}{\partial y}\right), \tag{3}$$

$$u\frac{\partial T}{\partial x}+v\frac{\partial T}{\partial y}=\alpha\frac{\partial^2 u}{\partial y^2}, \tag{4}$$

where *(u, v)* are the velocity components along the *(x, y) ax*es, ρ is the fluid density, μ is the coefficient of viscosity, k is the vertex viscosity, ν is the kinematic viscosity, j is the microrotation density, γ is the micropolar constant, N is the angular microrotation momentum, T is temperature, α is the thermal diffusivity, p is pressure and U_∞ is the free stream velocity. The corresponding boundary conditions for the problem are

$$u=U_w,\quad v=0,\quad N=n\left(\frac{\partial v}{\partial x}-\frac{\partial u}{\partial y}\right),\quad T=T_w(x),\quad at\ y=0, \tag{5}$$

$$u\to U_\infty,\quad N\to 0,\quad T\to T_\infty,\quad as\ y\to\infty, \tag{6}$$

where U_w is the stretching velocity and T_w is the surface temperature. For exponential stretching, the expression for U_∞, U_w and T_w are defined as

$$U_\infty=ae^{x/L},\qquad U_w=be^{x/L},\qquad T_w=T_\infty+ce^{x/L} \tag{7}$$

in which a and b are constant velocities, c is constant temperature and L is the reference length.

To convert Equations *(1)* to *(4)* into a nondimensional form we introduce the following similarity transformations

$$u=ae^{x/L}f'(\eta),\quad v=-\left(\frac{\nu a}{2L}\right)^{\frac{1}{2}}e^{x/2L}\left(f(\eta)+\eta f'(\eta)\right), \tag{8}$$

$$N=ae^{x/L}\frac{\eta}{y}M(\eta),\quad \theta=\frac{T-T_\infty}{T_w-T_\infty},\quad \eta=\left(\frac{a}{2\nu L}\right)^{\frac{1}{2}}e^{x/2L}y, \tag{9}$$

With the help of transformations given in Equations *(8)* and *(9)*, Equation *(1)* is identically satisfied and Equations *(2)* to *(4)* take the following form

$$f'''+\frac{1}{1+K}\left(ff''-2f'^2+2\right)+\frac{K}{1+K}M'=0, \tag{10}$$

$$M''+\frac{1}{\Lambda}(fM'-2f'M)-\frac{K\xi}{\Lambda\, Re}(M+f'')=0, \tag{11}$$

$$\theta''+\Pr(f\theta'-2f'\theta)=0, \tag{12}$$

in which $K=k/\mu$ is the micropolar parameter, $\Lambda=\gamma/\mu j$ is the micropolar coefficient, $Re=LU_\infty/2\nu$ is the non-similar Reynolds number, $Pr=\nu/\alpha$ is the Prandtl number and $\xi=\frac{L^2}{j}$. The boundary conditions in nondimensional form can be written as

$$f(0)=0,\quad f'(0)=\varepsilon,\quad f'\to 1,\ as\ \ \eta\to\infty, \tag{13}$$

$$M(0)=-nf''(0),\qquad M\to 0,\ as\ \ \eta\to\infty, \tag{14}$$

$$\theta(0)=1,\qquad \theta\to 0,\ as\ \ \eta\to\infty, \tag{15}$$

where $\varepsilon=b/a$. The skin friction coefficient and the local Nusselt numbers are obtained in dimensionless form as

$$Re^{1/2}\,C_f=\frac{1}{\varepsilon^2}(1+(1-n)K)f''(0),\quad \frac{Nu}{Re_x^{\frac{1}{2}}}=-\theta'(0). \tag{16}$$

where $Re_x^{\frac{1}{2}}=x^2U_\infty/2\nu L$ is local Reynolds number.

3. Numerical Solution of the Problem

To solve system of Equations *(10)* to *(12)* with the help of Keller-box scheme we first reduce the system into a first order one by taking the relations

$$s=f',\quad w=s',\quad P=M',\quad t=\theta' \tag{17}$$

with the help of Equation *(17)*, Equations *(10)* to *(12)* can be written as

$$w'+\frac{1}{1+K}(fw-2s^2+2)+\frac{K}{1+K}P=0, \tag{18}$$

$$P'+\frac{1}{\Lambda}(fP-2sM)-\frac{K\xi}{\Lambda\, Re}(M+w)=0, \tag{19}$$

$$t'+\Pr(ft-2s\theta)=0, \tag{20}$$

The corresponding boundary conditions take the form

$$f(0)=0,\quad s(0)=\varepsilon,\quad M(0)=-nf''(0),\quad \theta(0)=1, \tag{21}$$

$$s\to 1,\quad M\to 0,\quad \theta\to 0,\quad as\ \eta\to\infty \tag{22}$$

The above system of equations is first approximated by central differences and then those equations are linearized using Newton's method. The solution then can be obtained by applying block-elimination method over these linearized equations. The details of the procedure can be found in [29-31].

4. HAM Solutions

To validate the results obtained from Keller-box method an analytical solution of the problem is also provided with the help of HAM. For HAM solution we choose the initial guesses as

$$f_0(\eta)=(\varepsilon-1)+\eta-(\varepsilon-1)e^{-\eta} \tag{23}$$

$$M_0(\eta)=n(\varepsilon-1)e^{-\eta},\quad \theta_0(\eta)=e^{-\eta}, \tag{24}$$

The corresponding auxiliary linear operators are

$$L_f = \frac{d^3}{d\eta^3} + \frac{d^2}{d\eta^2}, \quad L_M = \frac{d^2}{d\eta^2} + \frac{d}{d\eta}, \quad L_\theta = \frac{d^2}{d\eta^2} + \frac{d}{d\eta} \quad (25)$$

which have the property

$$L_f[c_1 + c_2\eta + c_3 e^{-\eta}] = 0, \quad L_M[c_4 + c_5 e^{-\eta}] = 0,$$

$$L_\theta[c_6 + c_7 e^{-\eta}] = 0, \quad (26)$$

where $c_i (i = 1, \ldots, 7)$, are arbitrary constants. The 0th order deformation equations are defined as

$$(1-q)L_f\left[\hat{f}(\eta;q) - f_0(\eta)\right] = q\hbar_1 N_f\left[\hat{f}(\eta;q)\right], \quad (27)$$

$$(1-q)L_M\left[\hat{M}(\eta;q) - M_0(\eta)\right] = q\hbar_2 N_M\left[\hat{M}(\eta;q)\right], \quad (28)$$

$$(1-q)L_\theta\left[\hat{\theta}(\eta;q) - \theta_0(\eta)\right] = q\hbar_3 N_\theta\left[\hat{\theta}(\eta;q)\right], \quad (29)$$

in which

$$N_f\left[\hat{f}(\eta;q)\right] = \hat{f}''' + \frac{1}{1+K}\left(\hat{f}\,\hat{f}'' - 2\hat{f}'^2 + 2\right) + \frac{K}{1+K}\,\widehat{M}' \quad (30)$$

$$N_M\left[\hat{M}(\eta;q)\right] = \hat{M}'' + \frac{1}{\Lambda}\left(\hat{f}\,\hat{M}' - 2\hat{f}'\hat{M}\right) - \frac{K\xi}{\Lambda\, Re}\,(\hat{M} + \hat{f}'') \quad (31)$$

$$N_\theta\left[\hat{\theta}(\eta;q)\right] = \hat{\theta}'' + Pr\left(\hat{f}\,\hat{\theta}' - 2\hat{f}'\hat{\theta}\right) \quad (32)$$

The appropriate boundary conditions for the 0th order system are

$$\hat{f}(0;q) = 0, \quad \hat{f}'(\eta;q) = \varepsilon, \quad \widehat{f}'(\eta;q) \to 1, \ as\ \eta \to \infty, \quad (33)$$

$$\widehat{M}(0;q) = -n(\varepsilon - 1), \quad \widehat{M}(\eta;q) \to 0, \ as\ \eta \to \infty, \quad (34)$$

$$\hat{\theta}(0;q) = 1, \qquad \hat{\theta}(\eta;q) \to 0, \ as\ \eta \to \infty, \quad (35)$$

Further details of the HAM procedure can be found in [11, 12].

5. Results and Discussion

The convergence of HAM solution for velocity, microrotation and temperature have been discussed by plotting $\hbar$-curves for nondimensional f'', M'' and θ''. It is found that the admissible values of $\hbar$-curves are $-0.9 \le \hbar_1 \le -0.1$, $-1.25 \le \hbar_2 \le -0.3$ and $-1.5 \le \hbar_3 \le -0.25$ for velocity, microrotation and temperature profiles (Figures. *(1)-(3)*). Figures.*(4)* and *(5)* are plotted for comparison of the results obtained from numeric and HAM solution for nondimensional velocity f' for various values of microrotation parameter K and the stretching ratio ε. From these graphs it is clear that both the solutions are in good agreement. From Figure. *(4)* it is found that with the increase in the micropolar parameter K, the velocity profile f' decreases and also the boundary layer thickness reduces. Figure. *(5)* depicts the behavior of velocity profile f' with respect to the stretching ratio ε. It is observed from Figure. *(5)* that with an increase in the stretching ratio ε, the velocity profile f' also increases. The comparisons of analytical and numerical solutions obtained for the nondimensional microrotation profile M for different values of the micropolar parameter Λ and the stretching ratio ε are sketched in Figure. *(6)* and Figure. *(7)*. The observed settlement of the two solutions is acceptable. From Figure. *(6)* it is observed that as the micropolar parameter Λ increases, the microrotation velocity profile M is forced to decrease. Whereas, with increase in the stretching ratio ε, the microrotation profile M also increases. Figure. *(8)* is sketched to check the compatibility of the Keller-box and homotophy solutions obtained for the nondimensional heat transfer profile θ for different values of the Prandtl number Pr, from Figure. *(8)* it is observed that both the solutions are in agreement and that due to increase in the Prandtl number Pr the temperature profile θ decreases. Figure. *(9)* is designed to show the behavior of f' for different combinations of the micropolar parameter K and the stretching ratio ε. It is observed that for the stretching ratio $\varepsilon<0$ (shrinking sheet) an increase in the micropolar parameter K demands a decrease in the velocity profile f', while for the stretching ratio $\varepsilon>0$ $\left(\text{stretching sheet}\right)$ velocity profile f' has a dual behavior that is for the stretching ratio $\varepsilon<1$, an increase in the micropolar parameter K, the velocity profile f' decreases, whereas for the stretching ratio $\varepsilon>1$, with an increase in the micropolar parameter K, the velocity profile f' also increases. Figure.*(10)* is schemed to detect the manner revealed by the microrotation profile M when plotted for different combinations of the micropolar parameter Λ and the stretching ratio ε. It is observed that the behavior of micropolar parameter Λ for different values of the stretching ratio ε is similar to the behavior of the micropolar parameter K for different values of the stretching ratio ε over the microrotation profile M' (Figure. *(9))*.

The microrotation parameter M for various values of ξ against different Λ is plotted in Figure. (11). From Figure. (11) it is observed that with an increase in ξ, M increases. It is also observed from Figure. (11) that the rate of convergence for small Λ is much faster to that observed for a larger Λ. Figure. (12) is graphed to predict the influence of Re for different values of ε. It is observed that an increase in Re with $\varepsilon<1$ tends to decrease M, whereas for $\varepsilon>1$ the behavior is opposite. Figure. (13) is depicting over the effects of Pr over θ for different choices of ε. It is observed that temperature profile decreases with an increase in Pr the thermal boundary layer thickness also decreases and that the rate of convergence observed is minimizing with increase in ε. The coefficient of skin friction c_f for different values of K and ε against different Pr are shown in Figure. (14). It is observed that c_f increases with the increase in K and ε. The Nusselt number Nu for different values of Pr are shown in Figure. (15).

Table. (1) is prepared to observe the behavior of skin friction coefficient for different combinations of the parameters K, ε and Λ It is observed that skin friction decreases for all the parameters. *Table*. (2) is displaying the behavior of local Nusselt numbers for different combinations of the parameters Pr, ε and K. It seems that local Nusselt numbers increases with an increase in Pr and ε, whereas with an increase in K local Nusselt numbers decreases. From *Table*. (1) and *Table*. (2) it is obvious that the numerical solutions and the analytical solutions both are in excellent resemblance.

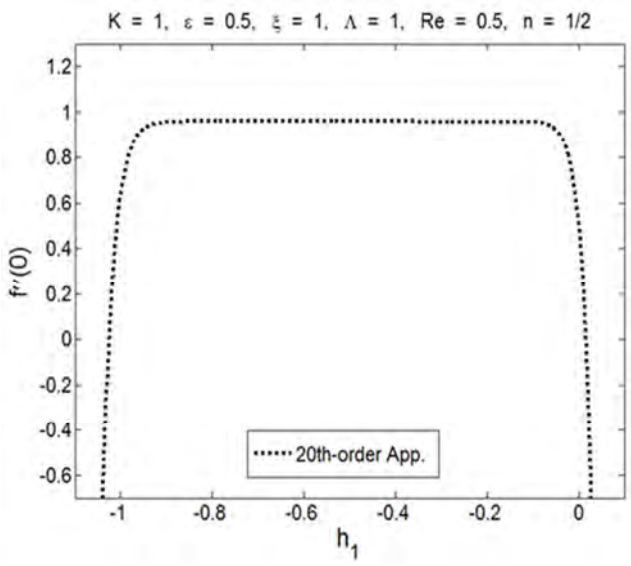

Figure 1. *ħ- curve for f.*

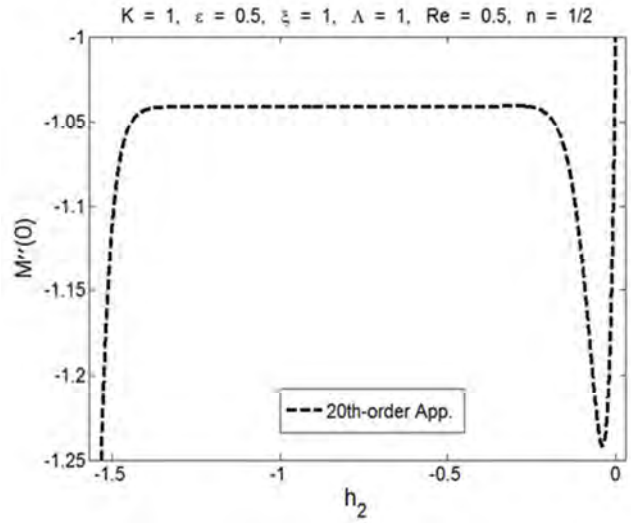

Figure 2. *ħ- curve for M.*

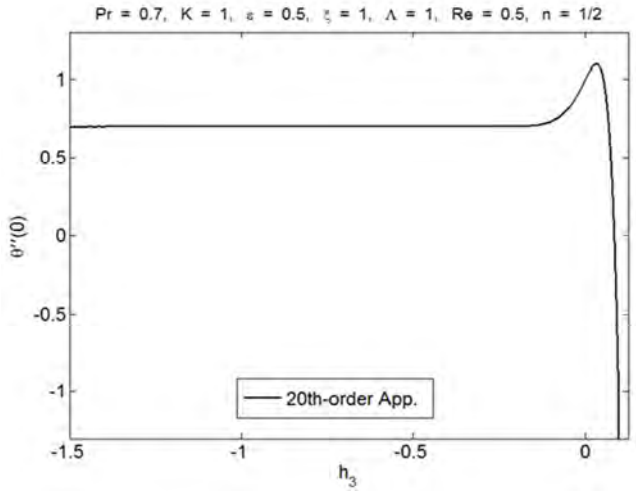

Figure 3. *ħ- curve for θ.*

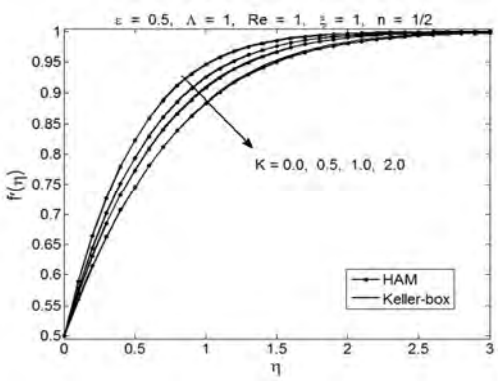

Figure 4. *Comparison of numerical and HAM solutions for different values of K over f'.*

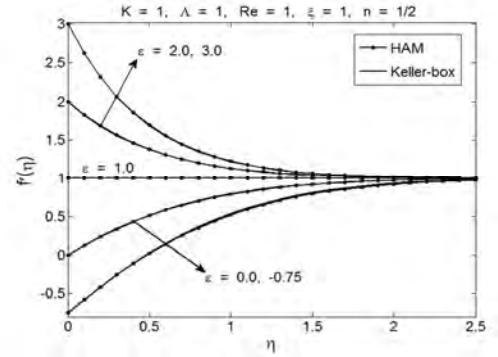

Figure 5. *Comparison of numerical and HAM solutions for different values of ε over f'.*

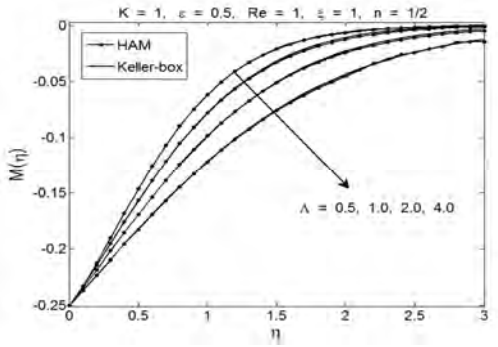

Figure 6. *Comparison of numerical and HAM solutions for different values of Λ over M.*

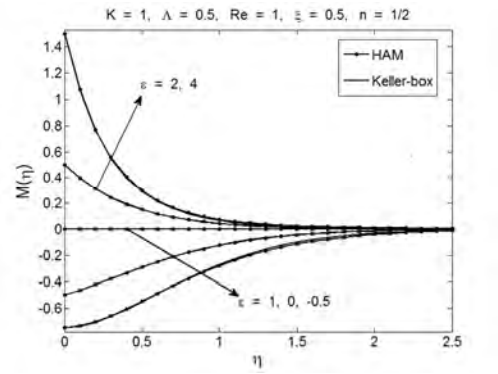

Figure 7. *Comparison of numerical and HAM solutions for different values of ε over M.*

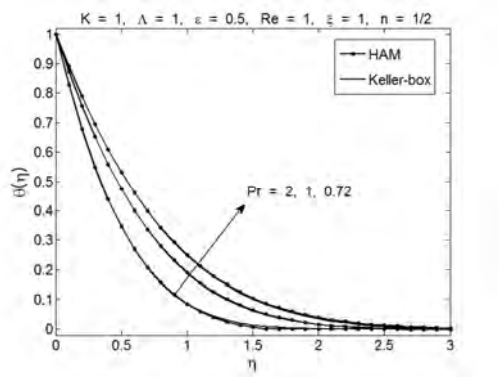

Figure 8. *Comparison of numerical and HAM solutions for different values of Pr over* θ.

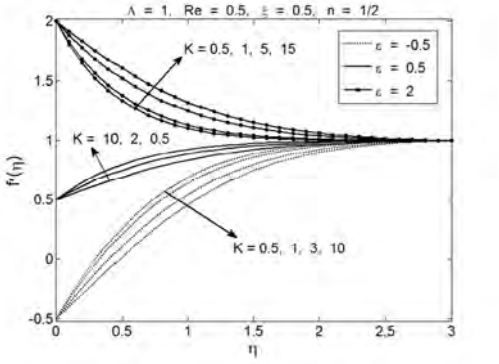

Figure 9. *Influence of K over* f' *for different values of ε.*

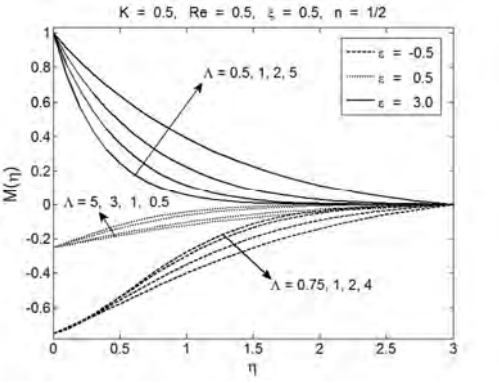

Figure 10. *Influence of* Λ *over* M *for different values of ε.*

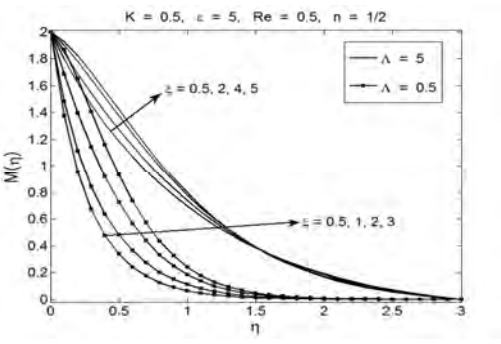

Figure 11. *Influence of* ξ *over* M *for different values of* Λ.

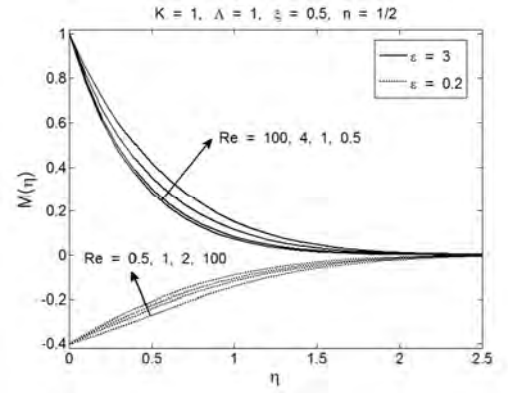

Figure 12. *Influence of Re over* M *for different values of ε.*

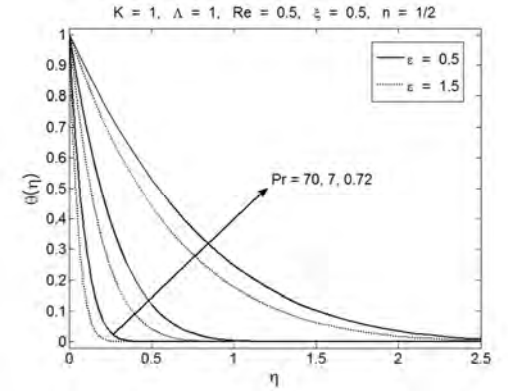

Figure 13. *Influence of Pr over* θ *for different values of ε.*

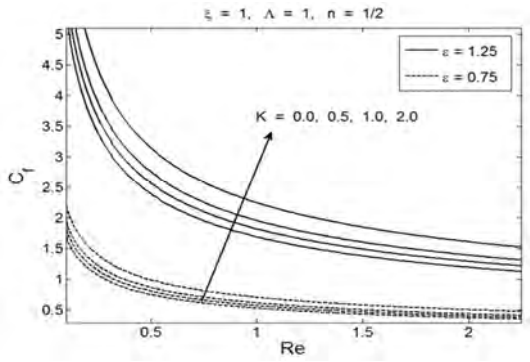

Figure 14. *Variation of Skin friction for different values of K and ε against Re.*

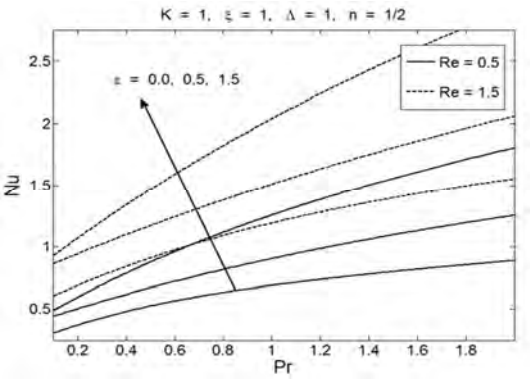

Figure 15. *Variation of Nusselt numbers for different values of Re and ε against Pr.*

Table 1. *Behavior of skin friction coefficient for Re=1,* $\xi = 1$.

		f´´(0)							
	Λ\ε	**-0.25**		**0.0**		**0.5**		**1.5**	
		K-b	**HAM**	**K-b**	**HAM**	**K-b**	**HAM**	**K-b**	**HAM**
	0.5	1.8317	1.8317	1.5854	1.5854	0.8997	0.8997	-1.0799	-1.0799
K = 0.2	1	1.8260	1.8260	1.5803	1.5803	0.8968	0.8968	-1.0767	-1.0767
	2	1.8200	1.8200	1.5749	1.5749	0.8938	0.8938	-1.0734	-1.0734
	0.5	1.6916	1.6916	1.4618	1.4618	0.8275	0.8275	-0.9899	-0.9899
K = 0.5	1	1.6845	1.6845	1.4548	1.4548	0.8231	0.8231	-0.9846	-0.9846
	2	1.6752	1.6752	1.4464	1.4464	0.8182	0.8182	-0.9789	-0.9789
	0.5	1.5180	1.5180	1.3099	1.3099	0.7399	0.7399	-0.8824	-0.8824
K = 1	1	1.5144	1.5144	1.3050	1.3050	0.7360	0.7360	-0.8768	-0.8768
	2	1.5063	1.5063	1.2969	1.2969	0.7308	0.7308	-0.8702	-0.8702
	0.5	1.2969	1.2969	1.1163	1.1163	0.6284	0.6284	-0.7469	-0.7469
K = 2	1	1.3011	1.3011	1.1173	1.1173	0.6272	0.6272	-0.7434	-0.7434
	2	1.2994	1.2994	1.1140	1.1140	0.6240	0.6240	-0.7382	-0.7382

Table 2. *Behavior of local Nusselt numbers for Λ=1, Re=1,* $\xi = 1$.

		-Ɵ´(0)							
	Pr\K	**0.0**		**0.5**		**1.0**		**2.0**	
		K-b	**HAM**	**K-b**	**HAM**	**K-b**	**HAM**	**K-b**	**HAM**
	0.72	1.1566	1.1566	1.1425	1.1425	1.1329	1.1329	1.1201	1.1201
ε = 0.5	1	1.3446	1.3446	1.3281	1.3281	1.3170	1.3170	1.3022	1.3022
	7	3.3150	3.3150	3.2817	3.2817	3.2598	3.2598	3.2315	3.2315
	10	3.9238	3.9238	3.8869	3.8869	3.8626	3.8626	3.8316	3.8316
	0.72	1.5313	1.5313	1.5438	1.5438	1.5522	1.5522	1.5632	1.5632
ε = 1.5	1	1.8199	1.8199	1.8341	1.8341	1.8435	1.8435	1.8556	1.8556
	7	5.0253	5.0253	5.0487	5.0487	5.0636	5.0636	5.0822	5.0822
	10	6.0490	6.0490	6.0741	6.0741	6.0901	6.0901	6.1099	6.1099
	0.72	2.4529	2.4529	2.5283	2.5283	2.5777	2.5777	2.6406	2.6406
ε = 5	1	2.9755	2.9755	3.0574	3.0574	3.1102	3.1102	3.1768	3.1768
	7	8.8622	8.8622	8.9774	8.9774	9.0492	9.0492	9.1379	9.1379
	10	10.7731	10.7731	10.8994	10.8994	10.9782	10.9782	11.0759	11.0759

References

[1] Crane LJ. Flow past a stretching plate. Z Angew Math Phys 1970; 21(4):645

[2] J. H. Merkin, V. Kumaran, The unsteady MHD boundary-layer flow on a shrinking sheet, Euro. J. Mech. B/Fluids 29 (2010) 357-363

[3] F. T. Akyildiz, D. A. Siginer, Existence results and numerical simulation of magneto hydrodynamic viscous flow over a shrinking sheet with suction, Math. Comp. Mod. 52 (2010) 346-354

[4] S. Nadeem, A. Hussain, M. Khan, HAM solutions for boundary layer flow in the region of the stagnation point towards a stretching sheet, Commun Nonlinear Sci Numer Simulat 15 (2010) 475-481

[5] N. A. Yacob, A. Ishak, I. Pop, Melting heat transfer in boundary layer stagnation-point flow towards a stretching/shrinking sheet in a micropolar fluid, Comp. Fluids 47 (2011) 16-21

[6] S. Nadeem, M. Awais, Thin film flow of an unsteady shrinking sheet through porous medium with variable viscosity, Phy. Letters A 372 (2008) 4965-4972

[7] C. Y. Wang, Stagnation flow towards a shrinking sheet, Int. J. Non-Linear Mech. 43 (2008) 377-382

[8] K. Bhattacharyya, G. C. Layek, Effects of suction/blowing on steady boundary layer stagnation-point flow and heat transfer towards a shrinking sheet with thermal radiation, Int. J. Heat Mass Tran. 54 (2011) 302-307

[9] Abdul Rehman, S. Nadeem, M. Y. Malik, Boundary layer stagnation-point flow of a third grade fluid over an exponentially stretching sheet, Braz. J. Chem. Eng. 30(3) (2013) 611-618

[10] Abdul Rehman, S. Nadeem, M. Y. Malik, Stagnation flow of couple stress nanofluid over an exponentially stretching sheet through a porous medium, J. Power Tech. 93(2) (2013) 122-132

[11] Sj. Liao, Notes on the homotopy analysis method: Some definitions and theorems, Commun. Nonlinear Sci. Numer. Simulat. 14 (2009) 983-997

[12] Sj. Liao, On the relationship between the homotopy analysis method and Euler transform, Commun. Nonlinear Sci. Numer. Simulat. 15 (2010) 1421-1431

[13] Abdul Rehman, S. Nadeem, Mixed convection heat transfer in micropolar nanofluid over a vertical slender cylinder, Chin. Phy. Lett. 29 (12) (2012) 124701-5

[14] Abdul Rehman, Saleem Iqbal, Syed Mohsin Raza, Axisymmetric Stagnation Flow of a Micropolar Fluid in a Moving Cylinder: An Analytical Solution, Fluid Mechanics, 2(1) (2016) 1-7.

[15] Abdul Rehman, S. Nadeem, S. Iqbal, M. Y. Malik, M. Naseer, Nanoparticle effect over the boundary layer flow over an exponentially stretching cylinder, J. Nano Engineering and Nano Systems (2014) 1-6.

[16] S. Nadeem, Abdul Rehman, Changhoon Lee, Jinho Lee, Boundary layer flow of second grade fluid in a cylinder with heat transfer, Mathematical Problems in Engineering, Volume 2012, Article ID 640289.

[17] S. Nadeem, Abdul Rehman, K. Vajravelu, J. Lee, C. Lee, Axisymmetric stagnation flow of a micropolar nanofluid in a moving cylinder, Volume 2012 (2012), Article ID 378259, 17 pages.

[18] A. K. Alomari, M. S. M. Noorani, R. M. Nazar, Approximate analytical solutions of the Klein-Gordon equation by means of the homotopy analysis method, J. Quality Measur. Ana. 4 (2008) 45-57.

[19] M. Y. Malik, M. Naseer, S. Nadeem, Abdul Rehman, The boundary layer flow of Casson nanofluid over a vertical exponentially stretching cylinder, Appl. Nano Sci. DOI: 10.1007/s13204-012-0267-0.

[20] S. Nadeem, Abdul Rehman, Mohamed Ali, The boundary layer flow and heat transfer of a nanofluid over a vertical slender cylinder, J. Nano Engineering and Nano Systems (2012) 1-9.

[21] S. Nadeem, Abdul Rehman, Axisymmetric stagnation flow of a nanofluid in a moving cylinder, Comp. Math. Mod. 24(2) (2013) 293-306.

[22] Abdul Rehman, S. Nadeem, Heat transfer analysis of the boundary layer flow over a vertical exponentially stretching cylinder, Global J. Sci. Fron. Res. 13(11) (2013) 73-85.

[23] Naheeda Iftikhar, Abdul Rehman, Peristaltic flow of an Eyring Prandtl fluid in a diverging tube with heat and mass transfer, International Journal of Heat and Mass Transfer 111 (2017) 667–676.

[24] Abdul Rehmana, S. Achakzai, S. Nadeem, S. Iqbal, Stagnation point flow of Eyring Powell fluid in a vertical cylinder with heat transfer, Journal of Power Technologies 96 (1) (2016) 57–62.

[25] Abdul Rehman, G. Farooq, I. Ahmed, M. Naseer, M. Zulfiqar, Boundary Layer Stagnation-Point Flow of Second Grade Fluid over an Exponentially Stretching Sheet, American J App Math Stat, 3(6) (2015) 211-219.

[26] Abdul Rehman, R. Bazai, S. Achakzai, S. Iqbal, M. Naseer, Boundary Layer Flow and Heat Transfer of Micropolar Fluid over a Vertical Exponentially Stretched Cylinder, App Comp Math, 4(6) (2015) 424-430.

[27] M. Y. Malik, M. Naseer, Abdul Rehman, Numerical study of convective heat transfer on the Power Law fluid over a vertical exponentially stretching cylinder, App Comp Math, 4(5), (2015) 346-350.

[28] M. Y. Malik, M. Naseer, S. Nadeem, Abdul Rehman, The boundary layer flow of hyperbolic tangent fluid over a vertical exponentially stretching cylinder, Alexandria Eng. J., 53 (2014) 747-750.

[29] H. B. Keller, T. Cebeci, Accurate numerical methods for boundary-layer flows. II: Two-dimensional flows, AIAA Journal 10 (1972) 1193-1199.

[30] H. B. Keller, Numerical methods in boundary layer theory, Annu. Rev. Fluid Mech. 10 (1978) 417-433.

[31] T. Cebeci, P. Bradshaw, Physical and Computational Aspects of Convective Heat Transfer, Springer-Verlag, New York, 1984.